

Solution of the plane contact problem between a finite-thickness laterally graded solid and a rigid stamp of an arbitrary tip-profile

O. ARSLAN

*Department of Mechanical Engineering, Eskisehir Osmangazi University,
Eskisehir 26480, Turkey, e-mail: oarслан@ogu.edu.tr*

A SINGULAR INTEGRAL EQUATION (SIE) APPROACH and a finite element method are developed for the solution of the frictional sliding contact problem between a finite-thickness laterally graded solid and a rigid stamp of an arbitrary tip-shape considering the plane strain assumption. An exponential shear modulus variation is introduced through the lateral direction. The field variables are obtained applying the Fourier transformation techniques on the governing partial differential equations. A surface displacement gradient is then utilized to derive a SIE of the second kind. A numerical solution of the SIE is performed by using a collation method and the Gauss quadrature integration techniques for the flat, triangular and circular stamp profiles. Finite element analyses (FEA) of the same contact problems are also performed upon selection of the augmented Lagrange contact-solver in ANSYS. For the incomplete (triangular and circular) stamp problems, an iterative algorithm is developed in order to obtain practically computational solutions for any desired contact lengths. Successful convergence of the SIE results and excellent consistency between the SIE and FEA results are attained, that indicate the reliability of both methods. The change in the thickness is shown to alter the contact behavior of the laterally graded solid significantly.

Key words: frictional sliding contact, laterally graded layer, singular integral equation, finite element method.

Copyright © 2019 by IPPT PAN, Warszawa

1. Introduction

GRADED MATERIALS ARE ADVANCE COMPOSITES which are designed to provide thermal, wear, corrosion or mechanical resistance depending on the engineering application, as well as their spatial material gradations reduce the risks of surface and interfacial failures by mitigating the stress levels. They are manufactured in a such a way that volume fractions of constituents are varied through the spatial coordinates via special deposition techniques [1, 2]. The variations in the mechanical properties such as Elastic modulus and Poisson's ratio can be measured through the beam deflection and ultrasonic pulse-echo techniques [3, 4]. As far as the contact mechanics of these materials are concerned, they tend to be more resistant and tolerant to the contact-related damages than homogeneous materials [5, 6]. Hence, contact behavior of miscellaneous types of graded materials should

be well understood to be able to design and characterize the most functional and resistant engineering materials. In literature there are an extensive amount of analytical and computational studies performed on the contact mechanics of graded materials. GULER and ERDOGAN [7, 8] obtained the SIE solution for the frictional sliding contact problem between a graded layer and a rigid stamp of an arbitrary surface profile. CHEN and CHEN [9] investigated a partial slip contact problem of a finite-thickness graded solid loaded by a rigid stamp of an arbitrary tip-shape. GUO *et al.* [10] put forward a closed form analytical solution for the adhesive contact between a rigid circular punch and a graded half-space. BORGI and COMEZ [11] studied the frictional receding contact problem between a homogeneous substrate and a graded layer of which the surface is loaded by a rigid circular punch. A rolling contact problem between two elastic solids coated with graded layers was discussed by GULER *et al.* [12]. COMEZ [13] considered a dynamic contact problem of a graded layer loaded by a moving rigid intender. CHOI and PAULINO [14] performed a thermoelastic contact mechanics analysis of a graded coating taking the frictional heat generation into account. Recently, ARSLAN and DAG [15] have presented SIE and computational solutions to the frictional sliding contact problem of orthotropic graded coatings under a rigid punch of an arbitrary profile. The effect of residual surface tension on the frictionless contact between a rigid cylindrical punch and a graded half-plane was investigated by VASU and BHANDAKKAR [16]. POLAT *et al.* [17] presented an analytical solution to the frictionless contact problem of a graded layer pressed by two dissimilar rigid flat stamps. COMEZ *et al.* [18] studied the receding contact problem of a graded layer resting on two quarter planes.

In all the aforementioned studies, spatial gradations of the mechanical properties are imposed through the thickness direction of elastic solids. On the other hand, CREMER and NEUSCHUTZ [19] declared that laterally graded hard coatings can be also deposited and characterized via the reactive magnetron sputtering technology. Moreover, functionality of some engineering systems is shown to be improved using laterally graded materials. For instance, laterally graded fracture fixation plates reduce stress shielding effects in bones, increase compressive stress at fractured bone interface leading to more quick healing, and also induce higher tensile stress in the uninjured portion of the bone preventing the development of distortional bone shapes [20, 21]. For thick-walled rotating vessels subjected to non-uniform inner and outer pressures, lateral gradation in mechanical properties is proved useful in the mitigation of stresses [22]. In literature few infinite half-plane solutions were carried out in order to comprehend the contact behavior of laterally graded materials. DAG *et al.* [23, 24] analyzed the frictional sliding contact of a laterally graded infinite half-plane loaded by a rigid intender of an arbitrary surface profile. CHEN and CHEN [25] formulated a solution for the contact problem between a circular rigid punch and an infinite half-plane with

shear modulus gradation through an arbitrary spatial direction. However, CHEN and CHEN [9] reported that the infinite half-plane solutions could not satisfactorily simulate the stresses generated in the finite-thickness test specimens, even if the thickness of the specimen seems sufficiently large (i.e., 10 times the contact length). Additionally, it can be inferred from the practical engineering applications [20–22] that the laterally graded materials are manufactured and adopted in the finite-thickness form, and contact mechanics problems of finite-thickness laterally graded solids have not been investigated so far.

In this study SIE-based and computational methods are developed for the frictional sliding contact problem of a laterally graded finite-thickness solid pressed by a rigid stamp of an arbitrary tip-shape. The plane strain assumption is considered in the problem. An exponential variation of the shear modulus is introduced through the lateral direction assuming constant Poisson's ratio. The graded layer is assumed to be fixed on a rigid foundation. Note that the elastic layer models on rigid foundation were wielded in various theoretical contact mechanics studies available in literature [9, 13, 26]. The field quantities in the present contact problem are obtained using the Fourier transformation techniques. The displacement gradient on the stamp surface is then reduced to a SIE of the second kind. The solution to the SIE is numerically enabled employing an expansion collocation technique and the Gauss quadrature integration techniques for the flat, triangular and circular stamp problems. On contrary to the infinite half-plane solutions in literature [23, 24] extra displacement boundary conditions are imposed to simulate the rigid substrate, which completely change the formulation and asymptotic analyses of the contact problem. Moreover, a recursive solution approach is employed in the solution of Cauchy's principal value integrals, although the previous half-plane studies [23–25] made use of Tricomi's approach. Computational solutions to the contact problems are also carried out in this study utilizing the FEA software ANSYS. The augmented Lagrange contact solver is selected in the solutions. Moreover, a new iterative algorithm is developed and integrated into the APDL (ANSYS Parametric Design Language) code to practically obtain computational solutions of the incomplete (triangular and circular) stamp problems for any desired contact lengths. The numerical results reveal successful convergence characteristics of the SIE method and excellent consistency between the SIE and FEA results. The influences of the problem parameters on the contact stresses, lateral stresses and contact forces are also demonstrated. The change in the layer thickness is shown to alter the contact and lateral stresses significantly, inferring that the infinite half-plane solutions cannot approximate the contact behavior of laterally graded finite-thickness materials well enough. Also considering that the advanced materials are substantially employed in the finite-thickness form, the results and procedures presented in this study can be used to enlighten the design and optimization of novel graded layers.

2. SIE method

The plane contact problem of a laterally graded elastic layer resting on a rigid foundation is considered in this study. The graded layer with the thickness h is in frictional contact with a rigid stamp of an arbitrary tip-shape as depicted in Fig. 1. The existence of the Coulomb dry friction between the surfaces of the graded layer and the rigid stamp results in the horizontal friction force $Q = \eta P$. Herein, η and P respectively stand for the coefficient of dry friction and the contact force. An exponential shear modulus variation is imposed on the elastic layer through the lateral y -direction. The flat, triangular and circular tip-shapes are considered for the rigid stamp whose endpoint locations are $y = a$ and $y = b$ as seen in Fig. 2. The flat stamp problem is a complete-type contact problem, and the triangular and circular stamp problems are incomplete-type contact problems. Note that the contact length $(b - a)$ and the contact force P are independent of each other in the complete contact problems and strongly dependent in the incomplete contact problems.

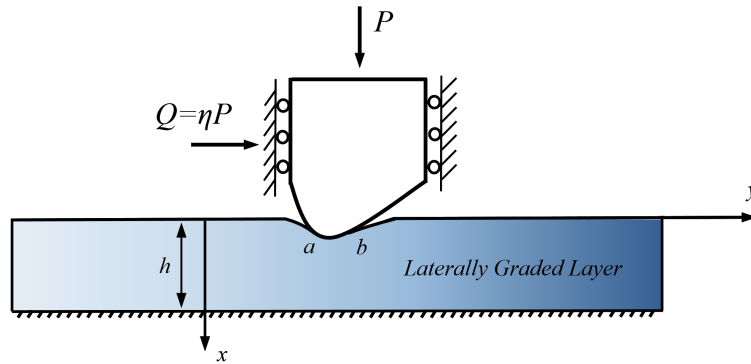


FIG. 1. Configuration of the problem.

2.1. Derivation of the SIE

Constitutive relations for the plane elasticity of a laterally graded medium can be stated as follows:

$$(2.1a) \quad \sigma_{xx} = \mu(y) \left(\frac{\kappa + 1}{\kappa - 1} \varepsilon_{xx} + \frac{3 - \kappa}{\kappa - 1} \varepsilon_{yy} \right),$$

$$(2.1b) \quad \sigma_{yy} = \mu(y) \left(\frac{3 - \kappa}{\kappa - 1} \varepsilon_{xx} + \frac{\kappa + 1}{\kappa - 1} \varepsilon_{yy} \right),$$

$$(2.1c) \quad \sigma_{xy} = 2\mu(y)\varepsilon_{xy},$$

ε_{ij} , σ_{ij} represent the strain components and the stress components, respectively. Note that $\kappa = 3 - 4\nu$ for the plane strain assumption. $\mu(y)$ is the shear modulus

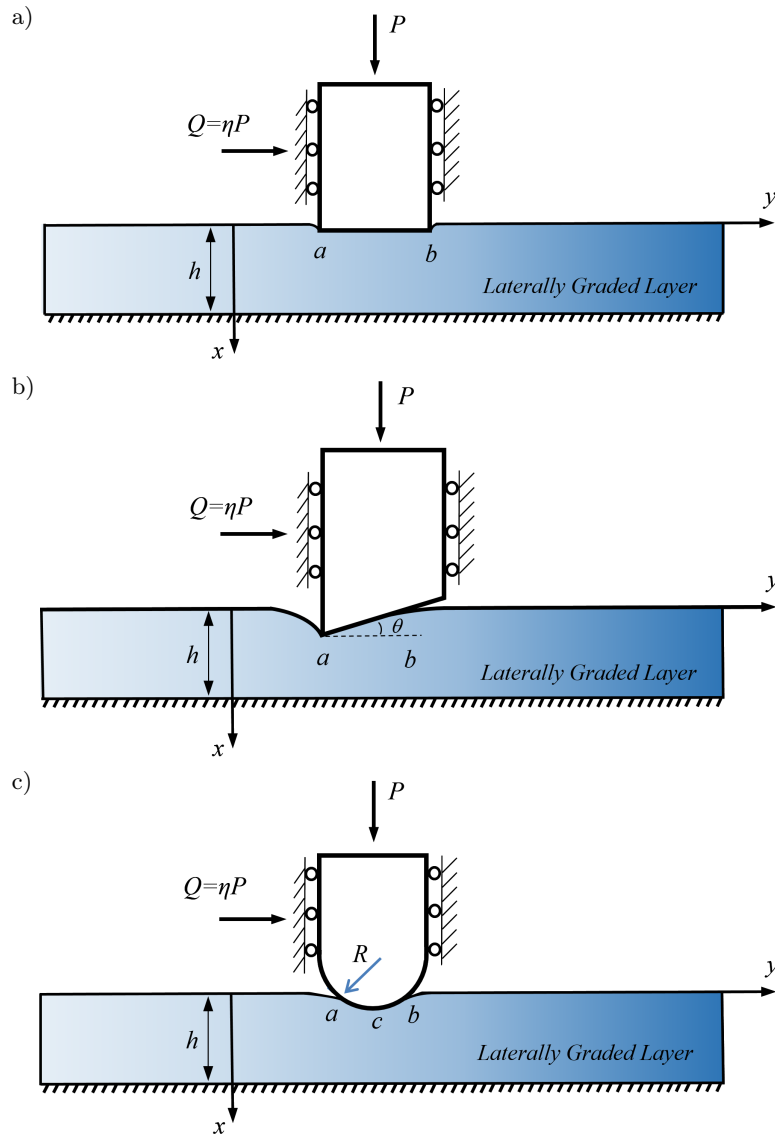


FIG. 2. Stamp geometries: (a) flat stamp problem, (b) triangular stamp problem, (c) circular stamp problem.

which is an exponentially varying function through the lateral y -direction:

$$(2.2) \quad \mu(y) = e^{\gamma y} \mu_0$$

where γ and μ_0 , respectively stand for the non-homogeneity parameter and the reference shear modulus at $y = 0$. The Poisson's ratio ν is assumed constant all through the elastic layer.

Under these considerations, the equilibrium equations are turned into a pair of partial differential equations in terms of the displacement components:

$$(2.3a) \quad \frac{\partial^2 u}{\partial y^2} + \frac{\kappa + 1}{\kappa - 1} \frac{\partial^2 u}{\partial x^2} + \frac{2}{\kappa - 1} \frac{\partial^2 v}{\partial x \partial y} + \gamma \frac{\partial u}{\partial y} + \gamma \frac{\partial v}{\partial x} = 0,$$

$$(2.3b) \quad \frac{\partial^2 v}{\partial x^2} + \frac{2}{\kappa - 1} \frac{\partial^2 u}{\partial x \partial y} + \frac{3 - \kappa}{\kappa - 1} \gamma \frac{\partial u}{\partial x} + \frac{\kappa + 1}{\kappa - 1} \gamma \frac{\partial v}{\partial y} + \frac{\kappa + 1}{\kappa - 1} \frac{\partial^2 v}{\partial y^2} = 0.$$

where u and v represent the displacement components in x and y directions, respectively.

The governing partial differential equations in Eqs. (2.3a-b) have to satisfy the boundary conditions of the problem given below:

$$(2.4a) \quad \sigma_{xx}(0, y) = \sigma_{xy}(0, y) = 0, \quad y < a, \quad y > b,$$

$$(2.4b) \quad \sigma_{xx}(0, y) = \sigma(y), \quad a < y < b,$$

$$(2.4c) \quad \sigma_{xy}(0, y) = \eta\sigma(y), \quad a < y < b,$$

$$(2.4d) \quad u(h, y) = v(h, y) = 0, \quad -\infty < y < \infty,$$

$$(2.4e) \quad \frac{\partial}{\partial y} u(0, y) = f(y), \quad a < y < b,$$

$$(2.4f) \quad \int_a^b \sigma_{xx}(0, y) dy = -P.$$

where $\sigma(y)$ is the contact pressure which is the primary unknown. $f(y)$ is a known function defining the tip-shape of the rigid stamp. In addition to the boundary conditions in Eqs. (2.4) all the field parameters must be bounded as $\sqrt{x^2 + y^2}$ tends to infinity, which is called the regularity condition.

Taking Fourier transformations of the displacement field in y :

$$(2.5a) \quad u(x, y) = \frac{1}{2\pi} \int_{-\infty}^{\infty} \sum_{j=1}^4 M_j e^{r_j x + i\rho y} d\rho,$$

$$(2.5b) \quad v(x, y) = \frac{1}{2\pi} \int_{-\infty}^{\infty} \sum_{j=1}^4 M_j N_j e^{r_j x + i\rho y} d\rho.$$

where the roots of the characteristic equation r_j and the function N_j read:

$$(2.6a) \quad r_1 = -r_3 = \frac{1}{\sqrt{2}} \sqrt{\delta_1 + \sqrt{\delta_1^2 - 4\delta_2}},$$

$$(2.6b) \quad r_2 = -r_4 = \frac{1}{\sqrt{2}} \sqrt{\delta_1 - \sqrt{\delta_1^2 - 4\delta_2}},$$

$$(2.6c) \quad \delta_1 = \frac{2\rho(\kappa + 1)(\gamma i - \rho) - \gamma^2(3 - \kappa)}{\kappa + 1},$$

$$(2.6d) \quad \delta_2 = -\rho^2(\gamma + i\rho)^2,$$

$$(2.6e) \quad N_j = \frac{(\kappa - 1)(\rho^2 - \gamma i\rho) - (\kappa + 1)r_j^2}{\{2i\rho + \gamma(\kappa - 1)\}r_j}.$$

M_j in Eq. (2.5) are determined using the boundary conditions conveyed in Eqs. (2.4a-c) in terms of the primary unknown function $\sigma(y)$ as follows:

$$(2.7a) \quad M_1 = p_1M_2 + p_2M_4,$$

$$(2.7b) \quad M_3 = p_3M_2 + p_4M_4,$$

$$(2.7c) \quad M_2 = \frac{\eta t_2 - t_4}{t_2t_3 - t_1t_4} \int_a^b \sigma(s)e^{-(\gamma+i\rho)s} ds,$$

$$(2.7d) \quad M_4 = \frac{t_3 - \eta t_1}{t_2t_3 - t_1t_4} \int_a^b \sigma(s)e^{-(\gamma+i\rho)s} ds.$$

where

$$(2.8a-b) \quad p_1 = \frac{N_3 - N_2}{N_1 - N_3} e^{(r_2-r_1)h}, \quad p_2 = \frac{N_3 - N_4}{N_1 - N_3} e^{(r_4-r_1)h},$$

$$(2.8c-d) \quad p_3 = \frac{N_1 - N_2}{N_3 - N_1} e^{(r_2-r_3)h}, \quad p_4 = \frac{N_1 - N_4}{N_3 - N_1} e^{(r_4-r_3)h},$$

$$(2.8d) \quad t_1 = \phi_1 p_1 + \phi_2 + \phi_3 p_3,$$

$$(2.8e) \quad t_2 = \phi_1 p_2 + \phi_4 + \phi_3 p_4,$$

$$(2.8f) \quad t_3 = i\theta_1 p_1 + i\theta_2 + i\theta_3 p_3,$$

$$(2.8g) \quad t_4 = i\theta_1 p_2 + i\theta_4 + i\theta_3 p_4,$$

$$(2.8i-j) \quad \phi_j = \mu \frac{(\kappa + 1)r_j + (3 - \kappa)N_j i\rho}{\kappa - 1}, \quad \theta_j = \mu(-N_j i r_j + \rho), \quad j = 1, \dots, 4.$$

The stress and strain fields are obtained by using the displacement field and the generalized Hook's law. Considering Eq. (2.5a) and Eqs. (2.7a-d), the displacement derivative in Eq. (2.4e) can be formulated rearranging the integral boundaries:

$$(2.9) \quad \frac{\partial}{\partial y} u(x, y) = \int_a^b k_1(x, y, s) \sigma_1(s) ds,$$

where

$$(2.10a) \quad k_1(x, y, s) = \frac{1}{2\pi} \int_0^{\infty} [K_{11}(\rho, x) \cos((y-s)\rho) + K_{12}(\rho, x) \sin((y-s)\rho)] d\rho,$$

$$(2.10b) \quad K_{11}(\rho, x) = \Gamma_1(\rho, x) + \Gamma_1(-\rho, x),$$

$$(2.10c) \quad K_{12}(\rho, x) = i\{\Gamma_1(\rho, x) - \Gamma_1(-\rho, x)\},$$

$$(2.10d) \quad \Gamma_1(\rho, x) = i\rho \frac{(\eta t_2 - t_4)(p_1 e^{r_1 x} + p_3 e^{r_3 x} + e^{r_2 x}) + (t_3 - \eta t_1)(p_2 e^{r_1 x} + p_4 e^{r_3 x} + e^{r_4 x})}{(t_2 t_3 - t_1 t_4)},$$

$$(2.10e) \quad \sigma_1(s) = \sigma(s) e^{-\gamma s}.$$

Singular behavior of the integrands as $\rho \rightarrow \infty$ are needed to be extracted from the kernel given in Eq. (2.10a). Hence, an asymptotic analysis of $K_{11}(\rho, x)$ and $K_{12}(\rho, x)$ is carried out starting with the asymptotic expansions of the characteristic equation roots (Eqs. 2.6a-b). Highly accurate asymptotic representations of the roots are obtained taking only the first two terms of the expansions into account:

$$(2.11a) \quad r_1^{\infty} = -r_3^{\infty} = |\rho| + 0.5C|\gamma| - 0.5\gamma i,$$

$$(2.11b) \quad r_2^{\infty} = -r_4^{\infty} = |\rho| - 0.5C|\gamma| - 0.5\gamma i,$$

where

$$(2.11c) \quad C = \sqrt{(3 - \kappa)/(\kappa + 1)}.$$

After substitution of Eqs. (2.11a-b) into Eqs. (2.10b-c), asymptotic expansions of $K_{11}(\rho, x)$ and $K_{12}(\rho, x)$ are enabled in the following forms:

$$(2.12a) \quad K_{11}^{\infty}(\rho, 0) = \left(f_{10} + \frac{f_{11}}{\rho} + \frac{f_{12}}{\rho^2} + \frac{f_{13}}{\rho^3} + \dots \right),$$

$$(2.12b) \quad K_{12}^{\infty}(\rho, 0) = \left(f_{20} + \frac{f_{21}}{\rho} + \frac{f_{22}}{\rho^2} + \frac{f_{23}}{\rho^3} + \dots \right),$$

where f_{ij} are the asymptotic expansion coefficients, given in Appendix A. In order to extract the singularities induced by the terms f_{10} , f_{20} , f_{11}/ρ and f_{21}/ρ as $\rho \rightarrow \infty$, they are added and subtracted from the expressions $K_{11}(\rho, x)$ and $K_{12}(\rho, x)$. After these operations and some algebraic manipulations, Eq. (2.9) turns into the following SIE of the second kind:

$$(2.13) \quad \frac{f_{10}}{2} \sigma_1(y) - \frac{f_{20}}{2\pi} \int_a^b \frac{\sigma_1(s)}{s-y} ds + \frac{1}{2\pi} \int_a^b K(s, y) \sigma_1(s) ds = f(y).$$

The SIE above consist of the Cauchy's principal value integral and a free term. The kernel $K(s, y)$ is available in Appendix A.

2.2. Numerical solution of the SIE

The solution to the SIE stated in Eq. (2.13) is carried out numerically starting with the definition of the normalizations below:

$$(2.14a) \quad y = \frac{b-a}{2}r + \frac{b+a}{2}, \quad -1 < r < 1,$$

$$(2.14b) \quad s = \frac{b-a}{2}t + \frac{b+a}{2}, \quad -1 < t < 1,$$

$$(2.14c-e) \quad \bar{\rho} = \frac{b-a}{2}\rho, \quad \bar{\gamma} = \frac{b-a}{2}\gamma, \quad \bar{h} = \frac{b-a}{2}h,$$

$$(2.14f-g) \quad \bar{A}_1 = \frac{b-a}{2}A_1, \quad \bar{A}_2 = \frac{b-a}{2}A_2,$$

$$(2.14h) \quad \sigma_1(y) = \sigma_1\left(\frac{b-a}{2}r + \frac{b+a}{2}\right) = \tilde{\sigma}(r).$$

2.2.1. Flat stamp problem. The displacement gradient on the surface of the flat stamp is expressed as:

$$(2.15) \quad f(y) = 0,$$

Taking Eqs. (2.14a-i) and Eq. (2.15) into account, the SIE (Eq. 2.13) and the equilibrium condition (Eq. 2.4f) are recast:

$$(2.16a) \quad \frac{f_{10}}{f_{20}}\bar{\sigma}(r) - \frac{1}{\pi} \int_{-1}^1 \frac{\bar{\sigma}(t)}{t-r} dt + \frac{1}{\pi f_{20}} \int_{-1}^1 \bar{K}(t, r) \bar{\sigma}(t) dt = 0,$$

$$(2.16b) \quad \int_{-1}^1 \bar{\sigma}(r) e^{\bar{\gamma}r + \bar{\gamma}^*} dr = -2,$$

where

$$(2.17a) \quad \bar{\gamma}^* = \frac{b+a}{2}\gamma,$$

$$(2.17b) \quad \bar{\sigma}(r) = \tilde{\sigma}(r)/(P/(b-a)),$$

The normalized kernel $\bar{K}(t, r)$ that appears in the normalized SIE (Eq. 2.16a) is given in Appendix A.

Referring to the theoretic analysis [27], the unknown function $\bar{\sigma}(r)$ can be represented by a series of the Jacobi polynomial regardless of the type of the elastic material and the tip-shape of the rigid punch:

$$(2.18) \quad \bar{\sigma}(r) = (1-r)^\alpha(1+r)^\beta \sum_{n=0}^{\infty} A_n P_n^{(\alpha,\beta)}(r), \quad -1 < r < 1,$$

where A_n ($n = 0, 1, 2, \dots$) are the unknown coefficients of the series expansion, and $P_n^{(\alpha,\beta)}(r)$ is the Jacobi polynomial of the order n . α and β are used to define the strengths of singularities of $\bar{\sigma}(r)$ at the contact ends $y = b$ and $y = a$, respectively:

$$(2.19a) \quad \alpha = \begin{cases} \varphi/\pi - 1, & \text{for } f_{10}/f_{20} \geq 0, \\ -\varphi/\pi, & \text{for } f_{10}/f_{20} < 0, \end{cases}$$

$$(2.19b) \quad \beta = \begin{cases} -\varphi/\pi, & \text{for } f_{10}/f_{20} \geq 0, \\ \varphi/\pi - 1, & \text{for } f_{10}/f_{20} < 0. \end{cases}$$

Truncating Eq. (2.18) at $n = N$ and substituting into the normalized SIE and equilibrium condition (Eqs. 2.16a-b), the following equations are obtained:

$$(2.20a) \quad \sum_{n=0}^N A_n F_n(r) = 0, \quad -1 < r < 1,$$

$$(2.20b) \quad \sum_{n=0}^N A_n R_n = -2,$$

where

$$(2.21a) \quad F_n(r) = \frac{f_{10}}{f_{20}}(1-r)^\alpha(1+r)^\beta P_n^{\alpha,\beta}(r) - \frac{L_n(r)}{\pi} + \frac{1}{f_{20}\pi} \int_{-1}^1 \bar{K}(t,r)(1-t)^\alpha(1-t)^\beta P_n^{(\alpha,\beta)}(t) dt,$$

$$(2.21b) \quad R_n = \int_{-1}^1 (1-r)^\alpha(1+r)^\beta P_n^{\alpha,\beta}(r) e^{\bar{\gamma}r+\gamma^*} dr.$$

The integrals stated in Eqs. (2.21) are computed through the Gauss quadrature integration techniques. The term $L_n(r)$ is the recursive solution of the Cauchy's principal value integral which is available in Appendix B.

The unknown coefficients A_n ($n = 0, \dots, N$) are computed by using $N + 1$ linear equations which consist of Eq. (2.20b) and collocation of Eq. (2.20a) at N roots of the Chebyshev polynomial the first kind given below:

$$(2.22) \quad r_i = \cos\left(\frac{\pi(2i-1)}{2N}\right), \quad i = 1, \dots, N.$$

Considering Eq. (2.20b) and the truncated form of Eq. (2.18) at $n = N$, the dimensionless contact stress for the flat stamp problem is formulated as follows:

$$(2.23) \quad \frac{\sigma\left(\frac{b-a}{2}r + \frac{b+a}{2}\right)}{P/(b-a)} = e^{(\tilde{\gamma}r + \gamma^*)}(1-r)^\alpha(1+r)^\beta \sum_{n=0}^N A_n P_n^{\alpha, \beta}(r).$$

2.2.2. Triangular stamp problem. The displacement gradient on the surface of the triangular stamp is expressed as:

$$(2.24) \quad f(y) = -\tan(\theta),$$

where θ is the inclination angle of the triangular stamp surface.

Taking Eqs. (2.14a-i) and Eq. (2.24) into account, the SIE (Eq. 2.13) and the equilibrium condition (Eq. 2.4f) are recast as:

$$(2.25a) \quad \frac{f_{10}}{f_{20}} \bar{\sigma}(r) - \frac{1}{\pi} \int_{-1}^1 \frac{\bar{\sigma}(t)}{t-r} dt + \frac{1}{\pi f_{20}} \int_{-1}^1 \bar{K}(t, r) \bar{\sigma}(t) dt = -2/(f_{20}\mu),$$

$$(2.25b) \quad \int_{-1}^1 \bar{\sigma}(r) e^{\tilde{\gamma}r + \gamma^*} dr = -2P(\mu \tan(\theta)(b-a)),$$

where

$$(2.26) \quad \bar{\sigma}(r) = \tilde{\sigma}(r)/(\mu \tan(\theta)).$$

The normalized kernel $\bar{K}(t, r)$ that appears in the normalized SIE (Eq. 2.25a) is given in Appendix A. The term γ^* is given in Eq. (2.17a).

$\bar{\sigma}(r)$ in Eq. (2.26) can be expressed by the series representation given in Eq. (2.18). The strengths of singularities of $\bar{\sigma}(r)$ are written for the triangular stamp case as:

$$(2.27a) \quad \alpha = \begin{cases} \varphi/\pi & \text{for } f_{10}/f_{20} \geq 0, \\ 1 - \varphi/\pi & \text{for } f_{10}/f_{20} < 0, \end{cases}$$

$$(2.27b) \quad \beta = \begin{cases} -\varphi/\pi & \text{for } f_{10}/f_{20} \geq 0, \\ \varphi/\pi - 1 & \text{for } f_{10}/f_{20} < 0. \end{cases}$$

Substituting the truncated form of $\bar{\sigma}(r)$ at $n = N$ into the normalized SIE and the equilibrium condition (Eqs. 2.25a-b), the following equations are obtained:

$$(2.28a) \quad \sum_{n=0}^N A_n F_n(r) = -2/(f_{20}\mu), \quad -1 < r < 1,$$

$$(2.28b) \quad \sum_{n=0}^N A_n R_n = -2P/(\mu \tan(\theta)(b-a)),$$

where $F_n(r)$ and R_n are given in Eqs. (2.21a-b).

The unknown coefficients A_n ($n = 0, \dots, N$) are computed by collocating Eq. (2.28a) at $N + 1$ roots of the Chebyshev polynomial of the first kind stated in Eq. (2.22).

Considering Eq. (2.28b) and the truncated form of Eq. (2.18) at $n = N$, the dimensionless contact stress for the triangular stamp problem is formulated as follows:

$$(2.29) \quad \frac{\sigma\left(\frac{b-a}{2}r + \frac{b+a}{2}\right)}{P/(b-a)} = -\frac{2e^{(\bar{\gamma}r+\gamma^*)}}{\sum_{n=0}^N A_n R_n} (1-r)^\alpha (1+r)^\beta \sum_{n=0}^N A_n P_n^{\alpha,\beta}(r).$$

2.2.3. Circular stamp problem. The displacement gradient on the surface of the circular stamp is expressed as:

$$(2.30) \quad f(y) = \frac{c-y}{R},$$

where R and c represent the radius and the centerline position of the circular stamp, respectively.

Taking Eqs. (2.14a-i) and Eq. (2.30) into account, the SIE (Eq. 2.13) and the equilibrium condition (Eq. 2.4f) are rearranged as:

$$(2.31a) \quad \frac{f_{10}}{f_{20}} \bar{\sigma}(r) - \frac{1}{\pi} \int_{-1}^1 \frac{\bar{\sigma}(t)}{t-r} dt + \frac{1}{\pi f_{20}} \int_{-1}^1 \bar{K}(t,r) \bar{\sigma}(t) dt = \frac{2c - (b-a)r - (b+a)}{\mu R f_{20}},$$

$$(2.31b) \quad \int_{-1}^1 \bar{\sigma}(r) e^{\bar{\gamma}r+\gamma^*} dr = -\frac{2P}{\mu(b-a)},$$

where

$$(2.32) \quad \bar{\sigma}(r) = \tilde{\sigma}(r)/\mu.$$

The normalized kernel $\bar{K}(t, r)$ that appears in the normalized SIE (Eq. 2.31a) is given in Appendix A. The term γ^* is given in Eq. (2.17a).

$\bar{\sigma}(r)$ in Eq. (2.32) can be expressed by the series representation given in Eq. (2.18). The strengths of singularities of $\bar{\sigma}(r)$ are written for the circular stamp case as:

$$(2.33a) \quad \alpha = \begin{cases} \varphi/\pi & \text{for } f_{10}/f_{20} \geq 0, \\ 1 - \varphi/\pi & \text{for } f_{10}/f_{20} < 0, \end{cases}$$

$$(2.33b) \quad \beta = \begin{cases} 1 - \varphi/\pi & \text{for } f_{10}/f_{20} \geq 0, \\ \varphi/\pi & \text{for } f_{10}/f_{20} < 0. \end{cases}$$

Substituting the truncated form of $\bar{\sigma}(r)$ at $n = N$ into the normalized SIE and equilibrium condition (Eqs. 2.31a-b), the following equations are obtained:

$$(2.34a) \quad \sum_{n=0}^N A_n F_n(r) = \frac{2c - (b-a)r - (b+a)}{\mu R f_{20}}, \quad -1 < r < 1,$$

$$(2.34b) \quad \sum_{n=0}^N A_n R_n = -\frac{2P}{\mu(b-a)},$$

where $F_n(r)$ and R_n are given in Eqs. (2.21a-b).

Expressing the right-hand side of Eq. (2.34a) in terms of the Jacobi polynomial of the first order, Eq. (2.34a) reduces to:

$$(2.35) \quad \sum_{n=0}^N A_n F_n(r) = \frac{(2c - (b-a)(2\alpha - 1) - (b+a))}{\mu R f_{20}} - \frac{2(b-a)}{\mu R f_{20}} P_1^{-\alpha, -\beta}(r), \quad -1 < r < 1.$$

The quantities a/R , b/R and c/R appearing in Eq. (2.34a) are not independent. One of them is dependent on the other two. In order to obtain a relationship between a/R , b/R and c/R , both sides of Eq. (2.35) are multiplied by $(1-r)^\alpha(1+r)^\beta$ then integrated from -1 to $+1$:

$$\begin{aligned}
(2.36) \quad \sum_{n=0}^N A_n \int_{-1}^1 F_n(r) (1-r)^{-\alpha} (1+r)^{-\beta} dr \\
= \frac{2c - (b-a)(2\alpha-1) - (b+a)}{\mu R f_{20}} \int_{-1}^1 (1-r)^{-\alpha} (1+r)^{-\beta} dr \\
- \frac{2(b-a)}{\mu R f_{20}} \int_{-1}^1 P_1^{-\alpha, -\beta}(r) (1-r)^{-\alpha} (1+r)^{-\beta} dr.
\end{aligned}$$

Note that the second integral on the right hand-side of Eq. (2.36) yields zero, and the first integral on the right-hand side is evaluated as:

$$(2.37) \quad \int_{-1}^1 (1-r)^{-\alpha} (1+r)^{-\beta} dr = \frac{\pi}{\sin(\pi\alpha)}, \quad \alpha + \beta = 1.$$

Rearranging Eq. (2.36):

$$(2.38) \quad \frac{\sin(\pi\alpha)}{\pi} \sum_{n=0}^N A_n M_n = \frac{2c - (b-a)(2\alpha-1) - (b+a)}{\mu R f_{20}},$$

where

$$(2.39a) \quad M_n = \frac{f_{10}}{f_{20}} \int_{-1}^1 P_n^{\alpha, \beta}(r) dr + \int_{-1}^1 (1-r)^{-\alpha} (1+r)^{-\beta} m_{1n}(r) dr,$$

$$(2.39b) \quad m_{1n}(r) = -\frac{1}{\pi} L_n(r) + \frac{1}{\pi f_{20}} \int_{-1}^1 \bar{K}(t, r) (1-r)^{\alpha} (1+r)^{\beta} P_n^{\alpha, \beta}(r) dt.$$

Considering Eq. (2.35) and Eq. (2.38) together, the following equation is formulated:

$$(2.40) \quad \sum_{n=0}^N A_n \left(F_n(r) - \frac{\sin(\pi\alpha)}{\pi} M_n \right) = -\frac{2(b-a)}{\mu R f_{20}} P_1^{-\alpha, -\beta}(r), \quad -1 < r < 1,$$

By using Eq. (2.38) the centerline position is obtained as:

$$(2.41) \quad \frac{c}{R} = \frac{f_{20} \sin(\pi\alpha) \mu}{2\pi} \sum_{n=0}^N A_n M_n + \frac{(b+a)}{2R} + \frac{(b-a)(2\alpha-1)}{2R}.$$

The unknown coefficients A_n ($n = 0, \dots, N$) are computed through the collocation of Eq. (2.40) at $N + 1$ roots of the Chebyshev polynomial of the first kind given in Eq. (2.22).

Considering Eq. (2.34b) and the truncated form of Eq. (2.18) at $n = N$, the dimensionless contact stress for the circular stamp problem is formulated as follows:

$$(2.42) \quad \frac{\sigma\left(\frac{b-a}{2}r + \frac{b+a}{2}\right)}{P/(b-a)} = -\frac{2e^{(\bar{\gamma}r+\gamma^*)}}{\sum_{n=0}^N A_n R_n} (1-r)^\alpha (1+r)^\beta \sum_{n=0}^N A_n P_n^{\alpha,\beta}(r).$$

3. Computational method

Computational solutions of the same contact problems are also carried out to be able to validate the SIE method and to reveal the effects of problem parameters on the contact and lateral stresses. The computational analyses are conducted utilizing the FEA software ANSYS upon selection of the augmented Lagrange contact-solver algorithm. Figure 3 illustrates the rectangular finite element model at which W , B and h respectively represent the width of the model, the contact length and the thickness of the graded layer. The width W is selected large enough to eliminate the effects of the model-edges on the displacement field of the contact region $h/W = 0.05$ and $h/B = 0.6$ are assigned in the model seen in Fig. 3. Equal sized 270 contact line elements (CONTA172) are

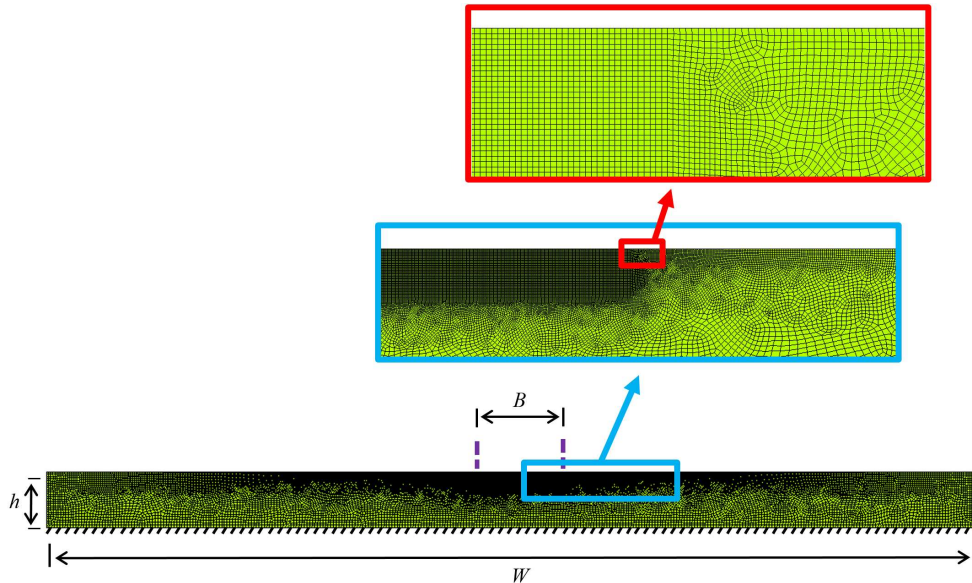


FIG. 3. Finite element model, $h/W = 0.05$, $h/B = 0.6$.

used to represent the contact surface of the graded layer. One rigid target element (TARGE169) is utilized for the rigid surfaces of flat and triangular stamps. Two rigid target elements are employed to model the circular stamp. Note that a flat stamp has two sharp ends and a triangular stamp has only one. A circular stamp has no sharp ends. The homogeneous finite element approach is used to introduce the lateral shear modulus variation through y -direction. In the homogeneous finite element approach, material properties of each finite element are defined at its geometric centroid. A total of 62348 triangular and quadrilateral finite elements (PLANE183) are employed in the discretization of the elastic layer seen in Fig. 3. In order to construct models having different h/B ratios, only the value of h is changed keeping the discretization of the model-boundaries unchanged. Relatively denser mesh refinement is adopted around the contact region to correctly get the stresses near the sharp contact ends and to obtain a smooth exponential variation of the shear modulus (see Eq. (2.2)). All the degree of freedoms of the bottom line nodes are fixed to zero in order to simulate the rigid foundation beneath the graded layer. The pivot points of the stamp are fixed to zero in rotation. Examining Section 2, the dimensionless contact stress $\sigma(y)/(P/(b-a))$ is seen independent of the inclination angle θ and the stamp radius R for the triangular and circular stamp problems, respectively. Note that defining the inclination angle θ as small as possible and R as large as possible

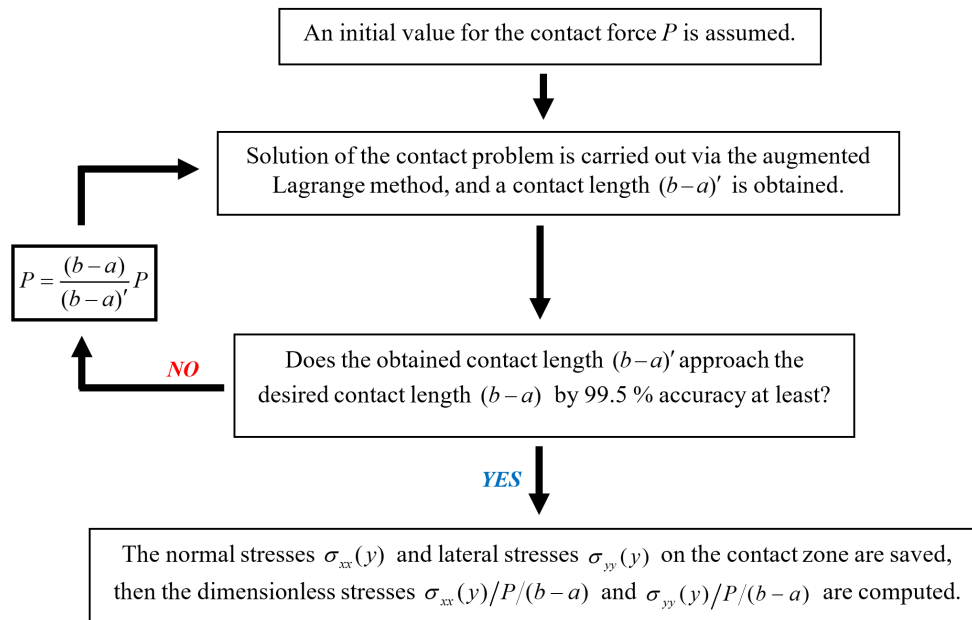


FIG. 4. Iterative procedure for the computational solution of the incomplete contact problems for a desired contact length $(b-a)$.

lead to small stamp indentations for which the computational solutions tend to converge better. Therefore, $\theta = \pi/36000$ and $(b-a)/R = 0.001$ are assigned in all the computational solutions of the triangular stamp and circular stamp problems, respectively. As previously mentioned, the contact length $(b-a)$ is independent of the contact force P in the complete contact problems (the flat stamp case). In the incomplete contact problems (the triangular and circular stamp cases) the contact length is significantly dependent on the contact force applied, and their relationships cannot be presumed. Hence, when a computational solution for an incomplete contact problem is required for a definite $h/(b-a)$ ratio, one should follow an iterative solution procedure. In this study, a new iterative algorithm is developed and integrated into the APDL code to practically get computational solutions for any desired contact lengths. The flowchart of the algorithm, which saves time and effort, can be seen in Fig. 4.

4. Numerical results

Parametric analyses are performed to prove the validity of the FEA and SIE method and to illustrate the influences of problem parameters on their results. The curves for the dimensionless contact stress $\sigma_{xx}(0, y)/(P/(b-a))$ and the dimensionless lateral stress $\sigma_{yy}/(P/(b-a))$ are presented with respect to dimensionless coordinate axis:

$$(4.1) \quad r = \frac{2y - (b+a)}{b-a}.$$

Note that $r = -1$ at the trailing end of the contact and $r = +1$ at the leading end of the contact for $\eta > 0$. In all the computations the Poisson's ratio ν is taken 0.3. The parameter γ^* in Eq. (2.17a) is assigned zero, causing that the origin of the $x-y$ coordinate system is located at the midpoint of the contact zone ($a = -b$). A negative coefficient of friction η indicates that the contact force Q is acting through the negative y -direction. Moreover, a positive normalized non-homogeneity parameter $\bar{\gamma}$ (Eq. 2.14d) implies that the layer stiffens in the positive y -direction. Thus, a negative $\bar{\gamma}$ makes the layer less stiff in the positive y -direction.

Table 1 tabulates the dimensionless contact stress $\sigma_{xx}/(P/(b-a))$ results generated for various values of the truncation number N to assess the convergence characteristics of the developed SIE method. As can be observed in this table, two-digit accuracy is attained when $N = 4$, and three-digit accuracy is attained when $N = 6$ for each combination of the problem parameters given. Hence, N is assigned 6 in all the computations of the SIE results. Figure 5 depicts the comparisons of the dimensionless contact stresses $\sigma_{xx}(0, y)/(P/(b-a))$ generated via the SIE method and FEA for the flat, triangular and circular stamp problems.

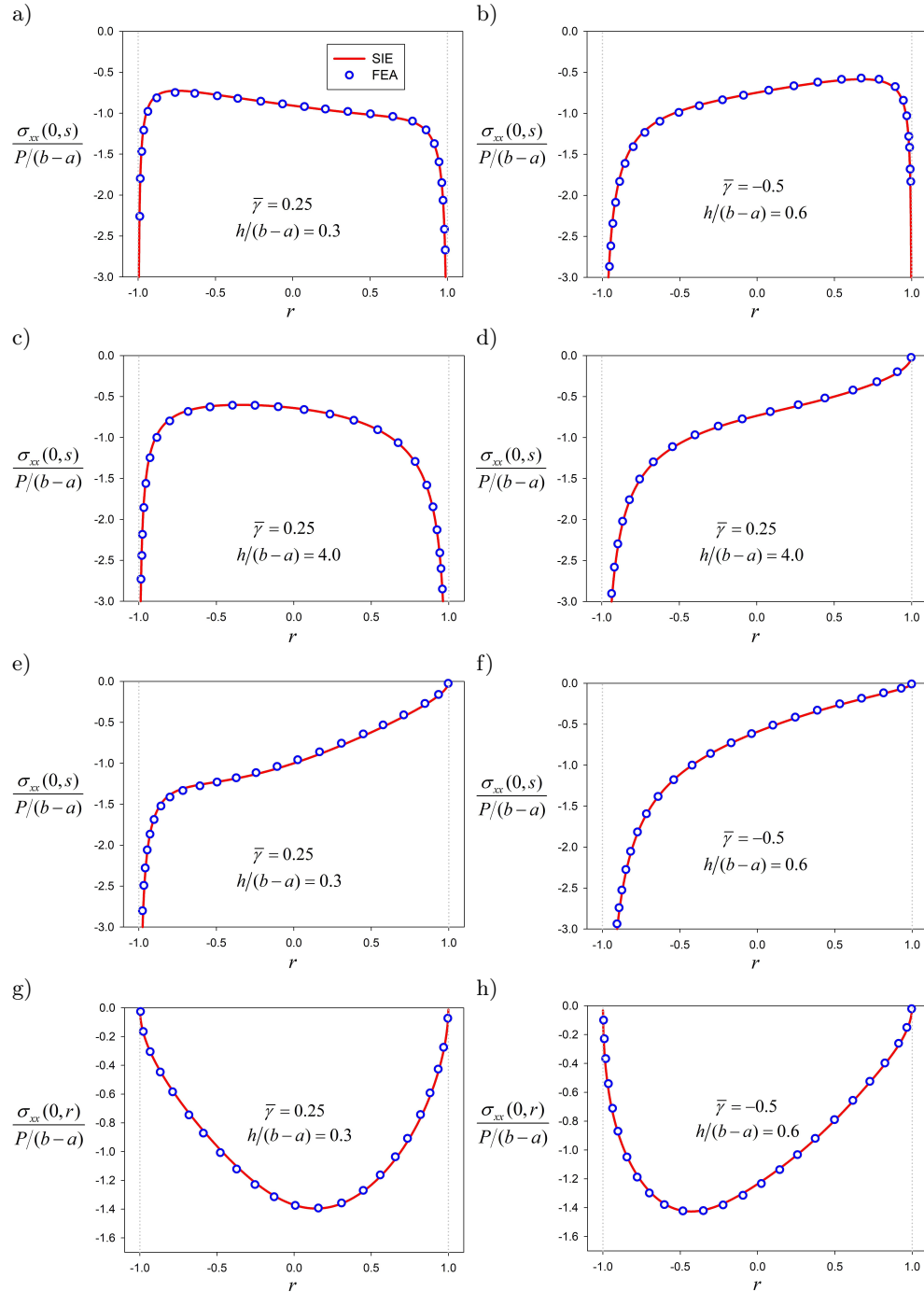


FIG. 5. Comparisons between FEA and SIE results: (a-c) flat stamp problem, (d-f) triangular stamp problem, (g-h) circular stamp problem, $\eta = 0.3$, $\bar{\gamma} = \gamma(b-a)/2$.

Table 1. Dimensionless contact stresses evaluated through the SIE method for an increasing truncation number N and various values of problem parameters considering the flat stamp problem, $\eta = 0.3$, $\gamma(b + a) = 0$, $r = (2y - (b + a))/(b - a)$, $h^* = h/(b - a)$, $\bar{\gamma} = \gamma(b - a)/2$.

	N	$\frac{\sigma_{xx}(0,y)}{P/(b-a)}$					
		$\bar{\gamma} = 0.25$			$\bar{\gamma} = 0.50$		
		$h^* = 0.3$	$h^* = 0.6$	$h^* = 1.2$	$h^* = 0.3$	$h^* = 0.6$	$h^* = 1.2$
$r = -0.6$	1	-0.657	-0.662	-0.661	-0.546	-0.546	-0.530
	2	-0.756	-0.722	-0.686	-0.629	-0.597	-0.551
	3	-0.750	-0.722	-0.688	-0.627	-0.601	-0.555
	4	-0.746	-0.715	-0.687	-0.625	-0.596	-0.555
	5	-0.746	-0.715	-0.687	-0.624	-0.596	-0.555
	6	-0.749	-0.715	-0.687	-0.627	-0.596	-0.554
	7	-0.749	-0.715	-0.687	-0.627	-0.596	-0.554
$r = 0.6$	1	-0.940	-0.932	-0.931	-1.052	-1.044	-1.051
	2	-1.030	-0.987	-0.954	-1.154	-1.106	-1.078
	3	-1.039	-0.988	-0.952	-1.158	-1.099	-1.071
	4	-1.034	-0.979	-0.951	-1.153	-1.090	-1.071
	5	-1.034	-0.979	-0.951	-1.153	-1.090	-1.071
	6	-1.037	-0.979	-0.951	-1.156	-1.090	-1.071
	7	-1.037	-0.979	-0.951	-1.156	-1.090	-1.071

The figure reveals that the results of two different methods agree with each other with a very good level of accuracy for various combinations of the normalized layer thickness $h/(b - a)$ and the normalized non-homogeneity parameter $\bar{\gamma}$.

Figure 6 demonstrates the deformed shapes of the computational solutions of the flat, triangular and circular stamp problems. Observing Fig. 6, the contact zone is discretized relatively denser to be able to correctly impose a smooth shear modulus gradation and capture stresses near the sharp contact edges.

In Figs. 7–9, the effects of problem parameters on the surface stresses of the flat stamp problem are presented. Figure 7 plots the effect of the normalized layer thickness $h/(b - a)$ on the dimensionless contact stress $\sigma_{xx}(0, y)/(P/(b - a))$ and lateral stress $\sigma_{yy}(0, y)/(P/(b - a))$ for the flat stamp problem. As the normalized layer thickness $h/(b - a)$ is increased from 0.3 to 4.0, the magnitude of the dimensionless contact stress $\sigma_{xx}(0, y)/(P/(b - a))$ increases near the contact edges but decreases significantly away from the contact edges. LAWN [6] experimentally introduced that the formation of Hertzian cone cracks are triggered by the surface lateral tensile stresses. As seen in Fig. 7b, the dimensionless lateral tensile stress $\sigma_{yy}(0, y)/(P/(b - a))$ increases when $h/(b - a)$ is raised from 0.3

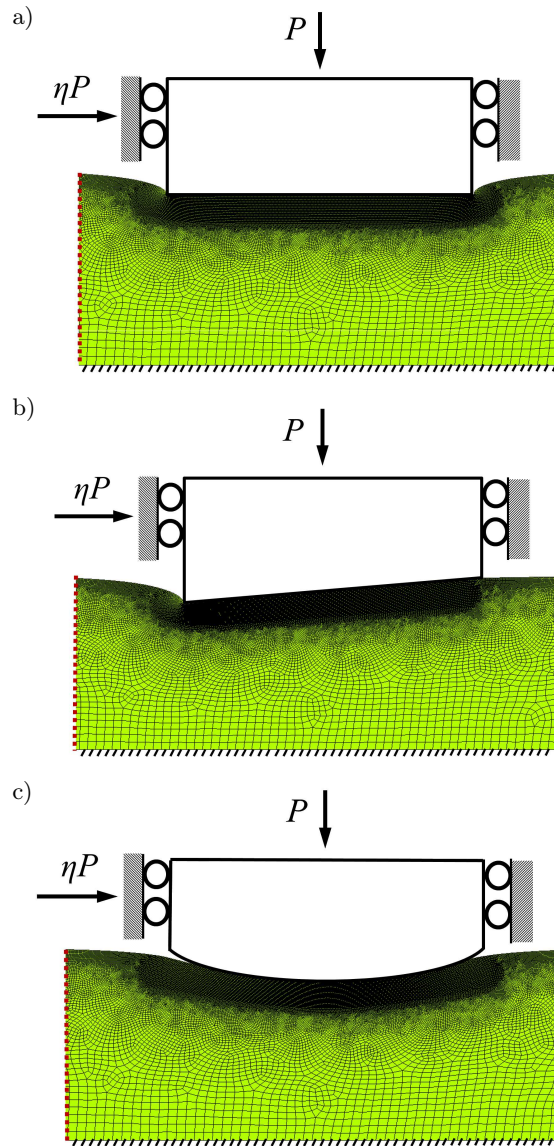


FIG. 6. Deformed contact regions: (a) flat stamp problem, (b) triangular stamp problem, (c) circular stamp problem, $\eta = 0.3$, $\bar{\gamma} = 0.25$, $h/(b-a) = 0.6$.

to 1.2, however decreases when $h/(b-a)$ is raised from 1.2 to 4.0. Figure 8 shows the effect of the normalized non-homogeneity parameter $\bar{\gamma}$ on the dimensionless contact stress $\sigma_{xx}(0, y)/(P/(b-a))$ and lateral stress $\sigma_{yy}(0, y)/(P/(b-a))$ for the flat stamp problem. As $\bar{\gamma}$ is increased from -0.5 to 0.5 , the plot of the dimensionless contact stress $\sigma_{xx}(0, y)/(P/(b-a))$ slants to the left, and the

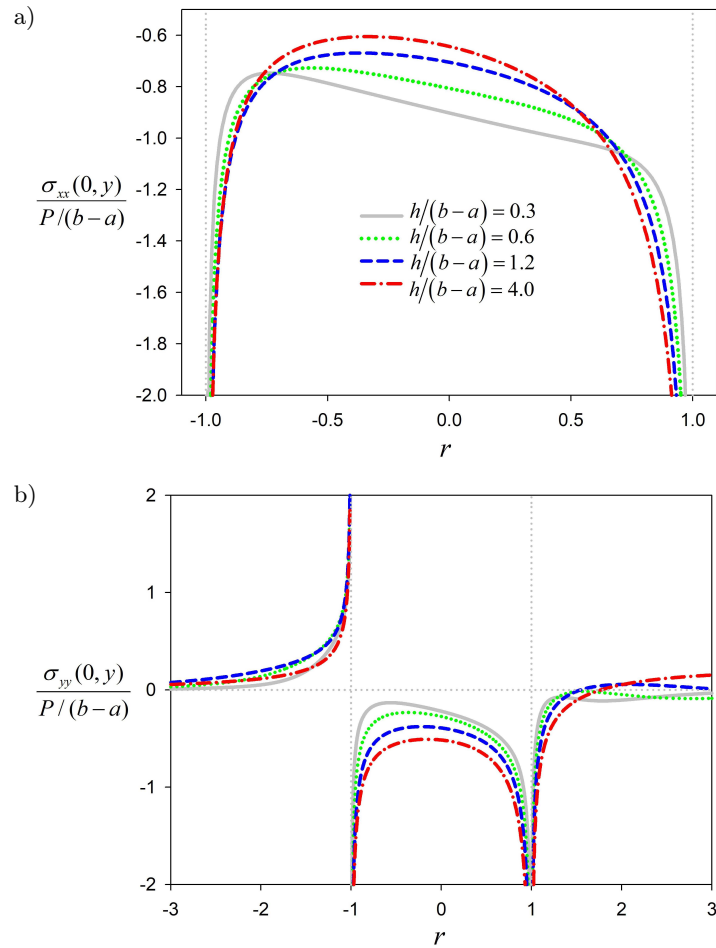


FIG. 7. Effect of the layer thickness on the dimensionless contact and lateral stresses for the flat stamp problem, $\eta = 0.3$, $\bar{\gamma} = 0.25$.

dimensionless lateral tensile stress $\sigma_{yy}(0, y)/(P/(b-a))$ decreases significantly. Figure 9 reveals the influences of the coefficient of friction η on the dimensionless contact stress $\sigma_{xx}(0, y)/(P/(b-a))$ and lateral stress $\sigma_{yy}(0, y)/(P/(b-a))$ for the flat stamp problem. Examining Fig. 9, the magnitude of the dimensionless contact stress $\sigma_{xx}(0, y)/(P/(b-a))$ increases slightly as the coefficient of friction η is increased from -0.6 to 0.6 . The effect of the coefficient of friction η on the dimensionless lateral tensile stress $\sigma_{yy}(0, y)/(P/(b-a))$ is seen quite significant.

In Figs. 10–12, the effects of problem parameters on the surface stresses of the triangular stamp problem are presented. The influences of the normalized

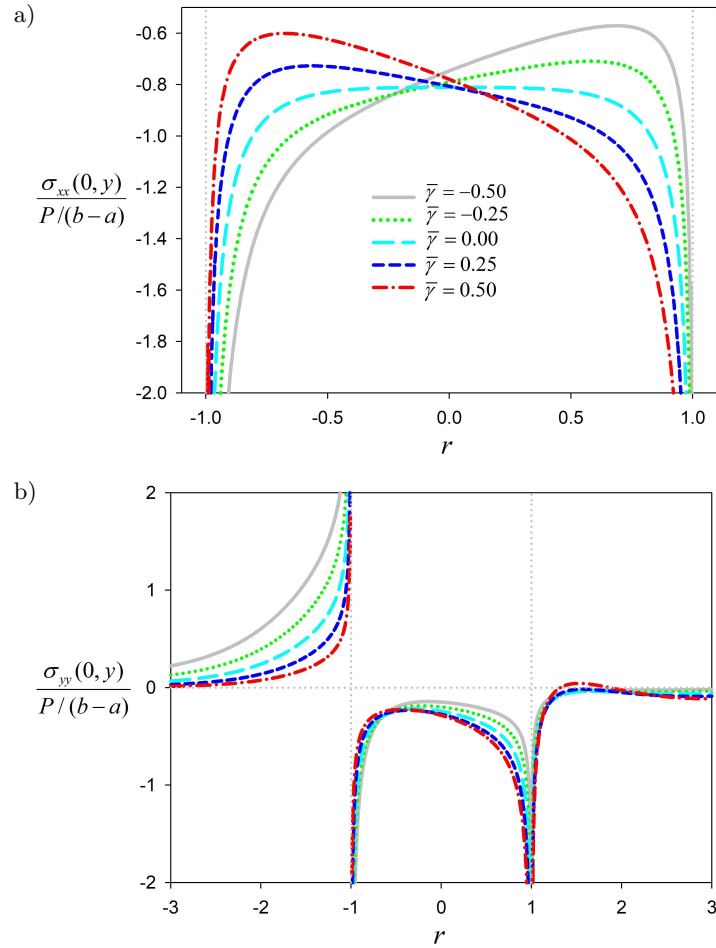


FIG. 8. Effect of the normalized non-homogeneity parameter on dimensionless contact and lateral stresses for the flat stamp problem, $\eta = 0.3$, $h/(b-a) = 0.6$.

layer thickness $h/(b-a)$ on the dimensionless contact stress $\sigma_{xx}(0, y)/(P/(b-a))$ and lateral stress $\sigma_{yy}(0, y)/(P/(b-a))$ are provided in Fig. 10 for the triangular stamp problem. It can be observed from Fig. 10a that the magnitude of the dimensionless contact stress $\sigma_{xx}(0, y)/(P/(b-a))$ ascends remarkably near the trailing end as the normalized layer thickness $h/(b-a)$ increases from 0.3 to 4.0. However, away from the trailing end, the magnitude of the dimensionless contact stress $\sigma_{xx}(0, y)/(P/(b-a))$ diminishes significantly especially in the middle zones of the contact. The effect of the normalized layer thickness $h/(b-a)$ on the dimensionless lateral tensile stress $\sigma_{yy}(0, y)/(P/(b-a))$ for the triangular stamp problem is similar to the flat stamp case. Figure 11 illustrates the influences

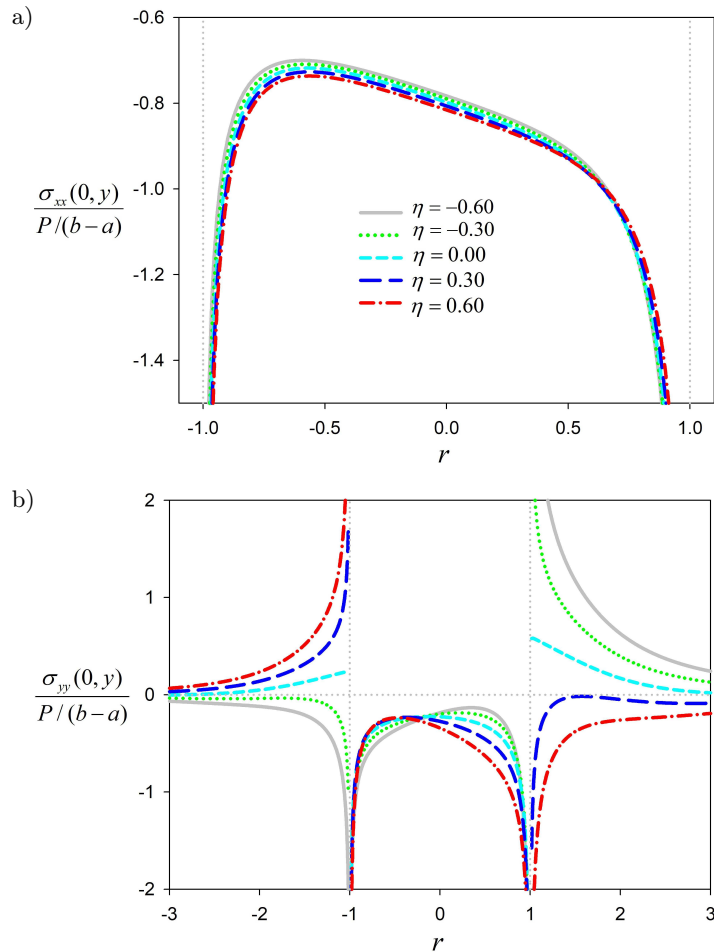


FIG. 9. Effect of the friction coefficient on the dimensionless contact and lateral stresses for the flat stamp problem, $\bar{\gamma} = 0.25$, $h/(b-a) = 0.6$.

of the normalized non-homogeneity parameter $\bar{\gamma}$ on the dimensionless contact stress $\sigma_{xx}(0, y)/(P/(b-a))$ and lateral stress $\sigma_{yy}(0, y)/(P/(b-a))$ for the triangular stamp problem. As seen in Fig. 11a, the magnitude of the dimensionless contact stress $\sigma_{xx}(0, y)/(P/(b-a))$ reduces significantly near the trailing end as the normalized non-homogeneity parameter $\bar{\gamma}$ is elevated from -0.5 to 0.5 . However, away from the trailing end, the magnitude of the dimensionless contact stress $\sigma_{xx}(0, y)/(P/(b-a))$ ascends very significantly. Observing Fig. 11b, the dimensionless lateral tensile stress $\sigma_{yy}(0, y)/(P/(b-a))$ dramatically decreases as the homogeneity parameter $\bar{\gamma}$ is increased from -0.5 to 0.5 . Figure 12 depicts the effects of the coefficient of friction η on the dimensionless contact stress

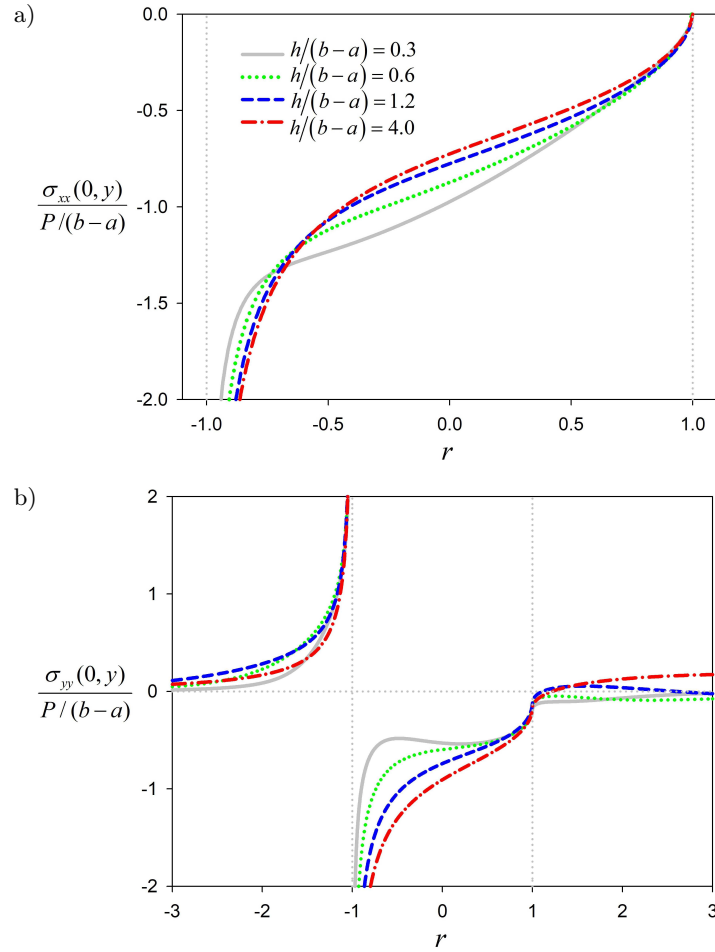


FIG. 10. Effect of the layer thickness on the dimensionless contact and lateral stresses for the triangular stamp problem, $\eta = 0.3$, $\bar{\gamma} = 0.25$.

$\sigma_{xx}(0, y)/(P/(b-a))$ and lateral stress $\sigma_{yy}(0, y)/(P/(b-a))$ for the triangular stamp problem. On contrary to the flat stamp problem, the magnitude of the dimensionless contact stress $\sigma_{xx}(0, y)/(P/(b-a))$ decreases slightly away from the trailing end as the coefficient of friction η is raised from -0.6 to 0.6 . As seen in Fig. 12b, the effect of the friction coefficient η on the dimensionless lateral tensile stress $\sigma_{yy}(0, y)/(P/(b-a))$ is very remarkable similar to the case of flat stamp problem.

In Figs. 13–15, the effects of problem parameters on the surface stresses of the circular stamp problem are presented. In Fig. 13, the influences of the normalized layer thickness $h/(b-a)$ on the dimensionless contact stress $\sigma_{xx}(0, y)/(P/(b-a))$

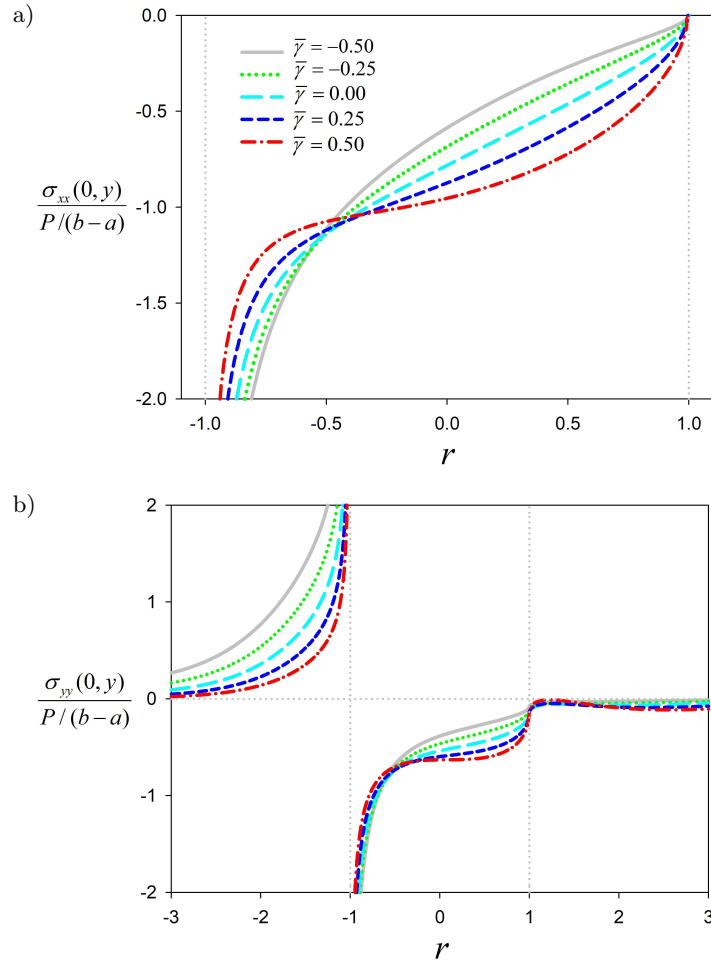


FIG. 11. Effect of the normalized non-homogeneity parameter on the dimensionless contact and lateral stresses for the triangular stamp problem, $\eta = 0.3$, $h/(b-a) = 0.6$.

and the lateral stress $\sigma_{yy}(0, y)/(P/(b-a))$ are depicted for the circular stamp problem. As seen in Fig. 13a, the magnitude of the dimensionless contact stress $\sigma_{xx}(0, y)/(P/(b-a))$ is decreased very remarkably when the normalized layer thickness $h/(b-a)$ is increased up to 1.2. However, no considerable change is observed in the dimensionless contact stress $\sigma_{xx}(0, y)/(P/(b-a))$ as the normalized layer thickness $h/(b-a)$ is increased above 1.2. Observing Fig. 13b, the dimensionless lateral tensile stress $\sigma_{yy}(0, y)/(P/(b-a))$ elevates remarkably, when the normalized layer thickness $h/(b-a)$ is increased up to 1.2. When the normalized layer thickness $h/(b-a)$ is increased above 1.2, the dimensionless lateral tensile stress $\sigma_{yy}(0, y)/(P/(b-a))$ tends to reduce. Figure 14 plots the

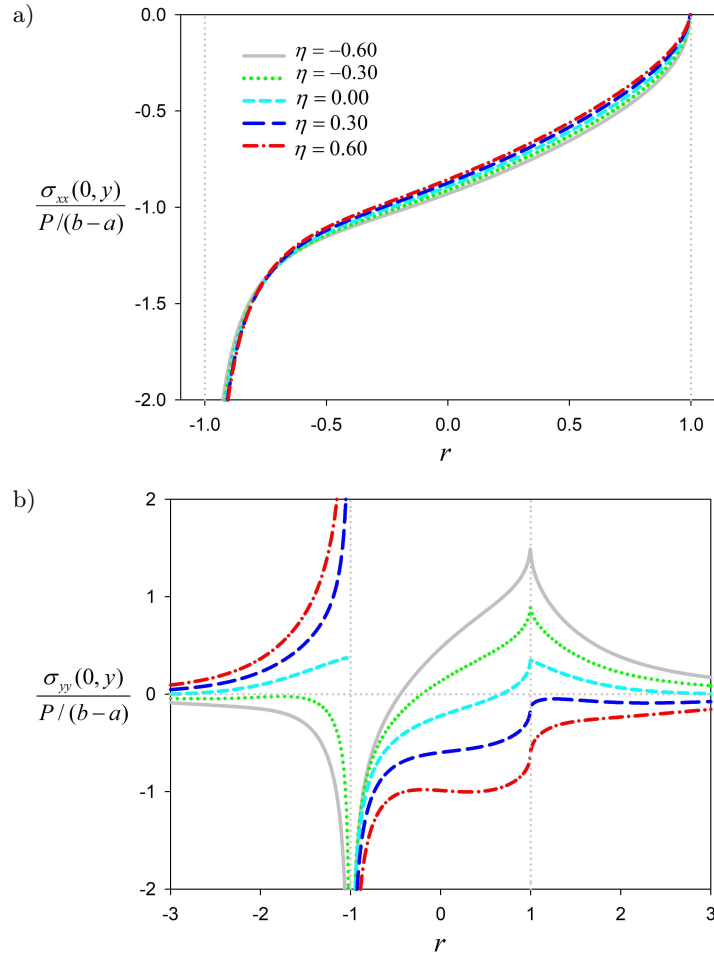


FIG. 12. Effect of the friction coefficient on the dimensionless contact and lateral stresses for the triangular stamp problem, $\bar{\gamma} = 0.25$, $h/(b-a) = 0.6$.

influences of the normalized non-homogeneity parameter $\bar{\gamma}$ on the dimensionless contact stress $\sigma_{xx}(0, y)/(P/(b-a))$ and lateral stress $\sigma_{yy}(0, y)/(P/(b-a))$ for the circular stamp problem. As the normalized non-homogeneity parameter $\bar{\gamma}$ is increased from -0.50 to 0.5 , the magnitude of the dimensionless contact stress $\sigma_{xx}(0, y)/(P/(b-a))$ diminishes significantly near the trailing end and increases remarkably near the leading end of the contact track. The dimensionless lateral tensile stress $\sigma_{yy}(0, y)/(P/(b-a))$ decreases evidently, as the normalized non-homogeneity parameter $\bar{\gamma}$ is increased from -0.50 to 0.5 . Figure 15 demonstrates the effects of the friction coefficient η on the dimensionless contact stress $\sigma_{xx}(0, y)/(P/(b-a))$ and lateral stress $\sigma_{yy}(0, y)/(P/(b-a))$ for the

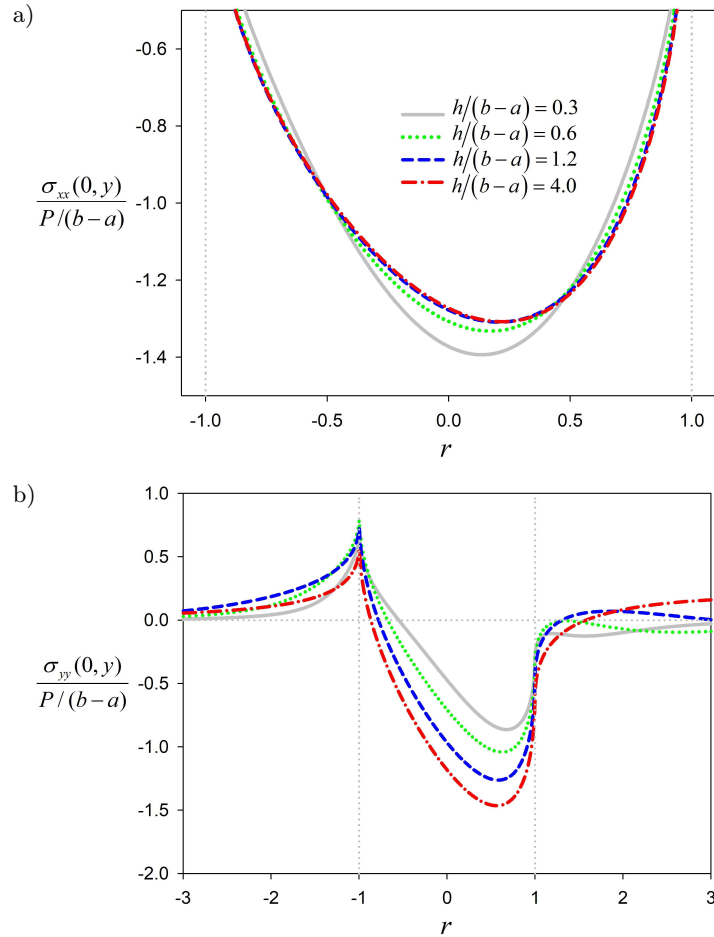


FIG. 13. Effect of the layer thickness on the dimensionless contact and lateral stresses for the circular stamp problem, $\eta = 0.3$, $\bar{\gamma} = 0.25$.

circular stamp problem. As the friction coefficient η increased from -0.6 to 0.6 , the magnitude of the dimensionless contact stress $\sigma_{xx}(0, y)/(P/(b-a))$ increases near the left edge but decreases near the right edge of the contact region. As can be examined from Fig. 15b, the effect of the friction coefficient η is very significant on the dimensionless lateral tensile stress $\sigma_{yy}(0, y)/(P/(b-a))$.

The triangular and circular stamp problems are incomplete contact problems for which the contact force P is strictly dependent on the contact length $(b-a)$. The influences of the problem parameters on the normalized contact force $P/(\mu(b-a)\tan(\theta))$ are tabulated in Table 2 which is created for the triangular stamp problem by considering Eq. (2.28b). Note that $P/(\mu(b-a)\tan(\theta))$ is independent of the inclination angle θ referring to Section 2.2.2. Observ-

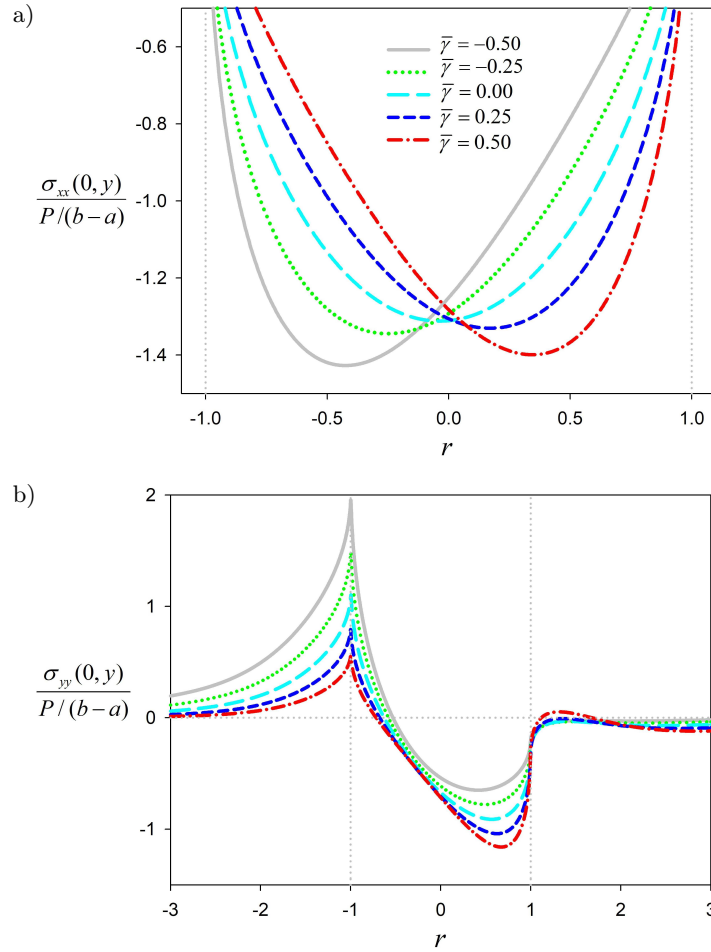


FIG. 14. Effect of the normalized non-homogeneity parameter on the dimensionless contact and lateral stresses for the circular stamp problem, $\eta = 0.3$, $h/(b - a) = 0.6$, $\bar{\gamma} = \gamma(b - a)/2$.

Table 2. Normalized contact forces evaluated through the SIE method for various values of problem parameters considering the triangular stamp problem, $\gamma(b + a) = 0$, $h^* = h/(b - a)$, $\bar{\gamma} = \gamma(b - a)/2$.

h^*	$P/(c_{660}(b - a) \tan(\theta))$					
	$\bar{\gamma} = 0.25$			$\bar{\gamma} = 0.50$		
	$\eta = 0.0$	$\eta = 0.3$	$\eta = 0.6$	$\eta = 0.0$	$\eta = 0.3$	$\eta = 0.6$
0.3	6.220	6.253	6.280	5.824	5.964	6.104
0.6	3.613	3.650	3.681	3.364	3.483	3.603
1.2	2.475	2.542	2.601	2.267	2.398	2.536

ing Table 2 the normalized contact force $P/(\mu(b - a) \tan(\theta))$ decreases significantly as the normalized layer thickness $h/(b - a)$ is increased from 0.3 to 1.2.

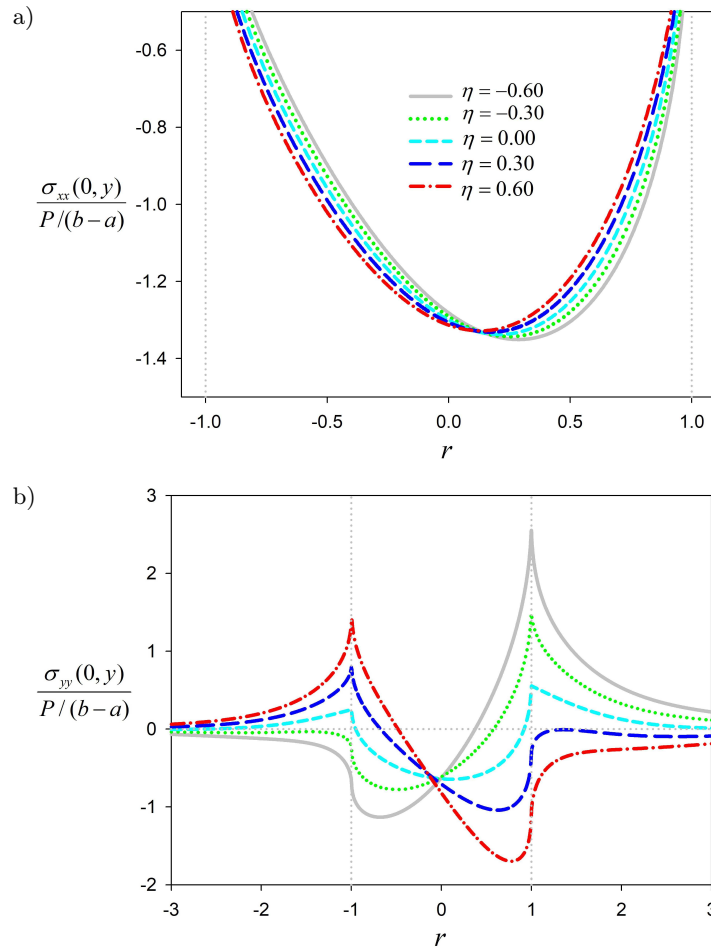


FIG. 15. Effect of the friction coefficient on the dimensionless contact and lateral stresses for the circular stamp problem, $\bar{\gamma} = 0.25$, $h/(b - a) = 0.6$.

$P/(\mu(b-a) \tan(\theta))$ also decreases as the normalized non-homogeneity parameter $\bar{\gamma}$ is raised from 0.25 to 0.5. Moreover, the increase in the friction coefficient η causes a slight elevation in the normalized contact force $P/(\mu(b-a) \tan(\theta))$ for each combination of the problem parameters. Examining Section 2.2.3 one can infer that the normalized contact force $P/(\mu(b-a))$ and the centerline position c/R for the circular stamp problem are dependent on the circular stamp radius R . Table 3 is generated to demonstrate the effects of the problem parameters on the normalized contact force $P/(\mu(b-a))$ for the circular stamp problem by considering Eq. (2.34b) and $(b-a)/R = 0.05$. As the degree of the positive material gradation is increased, the normalized contact force $P/(\mu(b-a))$ ascends slightly. When the normalized layer thickness $h/(b-a)$ is raised, the normalized

Table 3. Normalized contact forces evaluated through the SIE method for various values of problem parameters considering the circular stamp problem, $(b - a)/R = 0.05$, $\gamma(b + a) = 0$, $h^* = h/(b - a)$, $\bar{\gamma} = \gamma(b - a)/2$.

h^*	$P/(c_{660}/(b - a))$					
	$\bar{\gamma} = 0.25$			$\bar{\gamma} = 0.50$		
	$\eta = 0.0$	$\eta = 0.3$	$\eta = 0.6$	$\eta = 0.0$	$\eta = 0.3$	$\eta = 0.6$
0.3	0.01241	0.01251	0.01264	0.01267	0.01293	0.01325
0.6	0.00798	0.00808	0.00816	0.00817	0.00840	0.00859
1.2	0.00634	0.00641	0.00645	0.00656	0.00671	0.00683

Table 4. Centerline position evaluated through the SIE method for various values of problem parameters considering the circular stamp problem, $(b - a)/R = 0.05$, $\gamma(b + a) = 0$, $h^* = h/(b - a)$, $\bar{\gamma} = \gamma(b - a)/2$.

h^*	$(c/R) \times 10^5$					
	$\bar{\gamma} = 0.25$			$\bar{\gamma} = 0.50$		
	$\eta = 0.0$	$\eta = 0.3$	$\eta = 0.6$	$\eta = 0.0$	$\eta = 0.3$	$\eta = 0.6$
0.3	-0.150	-1.101	-1.863	-0.385	-1.018	-1.240
0.6	-2.324	2.587	7.856	-5.097	1.270	8.484
1.2	-10.891	2.509	16.520	-23.489	-6.519	12.010

contact force $P/(\mu(b - a))$ decreases remarkably for all the cases. The effects of problem parameters on the centerline position c/R of the circular stamp problem are also presented in Table 4 which is generated utilizing Eq. (2.41) for $(b - a)/R = 0.05$.

5. Concluding remarks

SIE and computational solutions for the sliding frictional contact problem between a laterally graded layer and a rigid stamp of an arbitrary tip-shape are performed in this study. Both complete and incomplete contact problems are investigated considering the plane strain assumption. A lateral spatial variation of the shear modulus is imposed on the elastic layer which is fixed on a rigid foundation. The field variables are obtained utilizing the Fourier transformation techniques. The non-deformable stamp profile defines a surface displacement gradient which is reduced to a SIE of the second kind. The SIE is solved numerically using a collocation method and the Gauss quadrature integration techniques. FEA of the same problem are carried out selecting the augmented Lagrange method in the software ANSYS. For the triangular and circular stamp problems, an iterative algorithm is developed to practically get computational stress results for

any desired contact lengths. Examining the parametric analyses presented for the flat, triangular and circular stamp problems, one can infer the followings:

The results of the SIE and FEA solutions have a high level of consistency, which indicates the reliability of both methods developed in this study. The successful convergence characteristics of the SIE results also exhibit the correct computation capability. Upon introducing positive lateral gradation ($\bar{\gamma} > 0$) in the layer, the lateral stresses can be mitigated significantly resulting in more resistant layers to contact loadings. This observation reveals the potential advantage of laterally graded layers over homogeneous layers, as far as their performance under contact loadings are considered. However, the resistance to contact loadings become poor when a negative lateral gradation ($\bar{\gamma} < 0$) is introduced in the layer. The friction coefficient is also shown as a significative factor on the contact and lateral stress curves. The level of the surface tensile stresses can be kept minimum by a simultaneous increase in the positive lateral gradation ($\bar{\gamma} > 0$) and decrease in the absolute value of the friction coefficient η . The curves of the dimensionless contact and lateral stresses are remarkably altered with the change of layer thickness. Observing the results showing the effect of layer thickness, a positively-graded layer in the thickness interval $0.6 < h/(b - a) < 1.2$ is more prone to surface cracking for all the stamp problems. *Hence, determination of layer thickness appears crucial in the design of laterally graded materials that are resistant to contact-induced damages.* Moreover, the solutions of infinite half-plane contact problems seem far from approximating the contact behavior of laterally graded layers with regard to the results that the effect of thickness is observed very significant on the contact and lateral stresses. Taking also into account that the advance materials are produced and adopted in the finite-thickness form, the results and procedures presented in this study can guide the design and analysis of new graded layers. In a future study, Stress Intensity Factors (SIFs) can be also formulated for the flat and triangular stamp problems to predict crack initiations due to asymptotic stresses at perfectly sharp contact ends.

Appendix A: Expressions in the SIE

Asymptotic expansion coefficients in Eq. (2.12) are obtained as:

$$(A.1) \quad f_{10} = -\frac{\eta(\kappa - 1)}{2\mu},$$

$$(A.2) \quad f_{11} = -\gamma \frac{\kappa^2 - 2\kappa - 3}{4\mu},$$

$$(A.3) \quad f_{12} = -\gamma^2 \frac{\eta(C^2 - 3)(\kappa^3 - \kappa^2 - 3\kappa - 1)}{32\mu},$$

$$(A.4) \quad f_{13} = -\gamma^3 \frac{\left[(C^2 - 3)\kappa^4 - 2(C^2 - 7)\kappa^3 - 8(C^2 + 3)\kappa^2 + 10(C^2 + 1)\kappa + 15C^2 + 51 \right]}{64\mu},$$

$$(A.5) \quad f_{20} = \frac{\kappa + 1}{2\mu},$$

$$(A.6) \quad f_{21} = -\frac{\eta\gamma(\kappa - 1)^2}{4\mu},$$

$$(A.7) \quad f_{22} = \gamma^2 \frac{(C^2 - 3)\kappa^3 + (C^2 + 13)\kappa^2 - (5C^2 + 9)\kappa - 5C^2 - 25}{32\mu},$$

$$(A.8) \quad f_{23} = \gamma^3 \frac{\eta(3 - C^2)(\kappa^4 - 2\kappa^3 - 2\kappa^2 + 2\kappa + 1)}{64\mu}.$$

The kernel $K(s, y)$ in Eq. (2.13) can be expressed as:

$$(A.9) \quad K(s, y) = \int_0^{A_1} (K_{11}(\rho, 0) - f_{10}) \cos((y-s)\rho) d\rho \\ + \int_{A_1}^{\infty} \left(\frac{f_{12}}{\rho^2} + \frac{f_{13}}{\rho^3} + \dots \right) \cos((y-s)\rho) d\rho - f_{11} Ci(|A_1(s-y)|) - \frac{\pi}{2} f_{21} \text{sign}(s-y) \\ + \int_0^{A_2} \left(K_{12}(\rho, 0) - f_{20} - \frac{f_{21}}{\rho} \right) \sin((y-s)\rho) d\rho \\ + \int_{A_2}^{\infty} \left(\frac{f_{22}}{\rho^2} + \frac{f_{23}}{\rho^3} + \dots \right) \sin((y-s)\rho) d\rho$$

where A_1 and A_2 are integration cut-off points. Ci is the cosine integral.

The normalized kernel $\bar{K}(t, r)$ that appears in Eq. (2.16a), Eq. (2.25a) and Eq. (2.31a) is stated as:

$$(A.10) \quad \bar{K}(t, r) = \int_0^{\bar{A}_1} (\bar{K}_{11}(\bar{\rho}, 0) - f_{10}) \cos((r-t)\bar{\rho}) d\bar{\rho} \\ + \int_{\bar{A}_1}^{\infty} \left(\frac{\bar{f}_{12}}{\bar{\rho}^2} + \frac{\bar{f}_{13}}{\bar{\rho}^3} + \dots \right) \cos((r-t)\bar{\rho}) d\bar{\rho} - \bar{f}_{11} Ci(|\bar{A}_1(t-r)|) - \frac{\pi}{2} \bar{f}_{21} \text{sign}(t-r) \\ + \int_0^{\bar{A}_2} \left(\bar{K}_{12}(\bar{\rho}, 0) - \bar{f}_{20} - \frac{\bar{f}_{21}}{\bar{\rho}} \right) \sin((r-t)\bar{\rho}) d\bar{\rho} + \int_{\bar{A}_2}^{\infty} \left(\frac{\bar{f}_{22}}{\bar{\rho}^2} + \frac{\bar{f}_{23}}{\bar{\rho}^3} + \dots \right) \sin((r-t)\bar{\rho}) d\bar{\rho}$$

where

$$(A.11) \quad K_{11}(\rho) = K_{11}\left(\frac{2}{b-a}\bar{\rho}\right) = \bar{K}_{11}(\bar{\rho}),$$

$$(A.12) \quad K_{12}(\rho) = K_{12}\left(\frac{2}{b-a}\bar{\rho}\right) = \bar{K}_{12}(\bar{\rho}),$$

$$(A.13) \quad \bar{f}_{ij} = \left(\frac{b-a}{2}\right)^j f_{ij} \quad (i = 1, 2, j = 0, 1, \dots)$$

Appendix B: Recursive solution of the Cauchy principal value integral

The recursive solution of the Cauchy principal value integral $L_n(r)$ is stated as follows [28]:

$$(B.1) \quad L_n(r) = \frac{1}{P_{n-1}^{(\alpha,\beta)}(r)} \left(P_n^{(\alpha,\beta)}(r) L_{n-1}(r) + \frac{\theta_{n-1}}{G_{n-1}} \right), \quad n = 1, 2, \dots,$$

$$(B.2) \quad G_n = \frac{2(n+1)(\alpha+\beta+n+1)}{(\alpha+\beta+2n+1)(\alpha+\beta+2n+2)}, \quad n = 0, 1, 2, \dots,$$

$$(B.3) \quad \theta_n = \frac{2^{\alpha+\beta+1} \Gamma(n+\alpha+1) \Gamma(n+\beta+1)}{(2n+\alpha+\beta+1)n! \Gamma(n+\alpha+\beta+1)}, \quad n = 1, 2, \dots,$$

$$(B.4) \quad L_0(r) = \frac{\pi}{\sin(\pi\alpha)} \times \begin{cases} (-r+1)^\alpha (r+1)^\beta \cos(\pi\alpha) & \text{for flat stamp,} \\ (-r+1)^\alpha (r+1)^\beta \cos(\pi\alpha) - 1 & \text{for triangular stamp,} \\ (-r+1)^\alpha (r+1)^\beta \cos(\pi\alpha) - r + \alpha - \beta & \text{for circular stamp.} \end{cases}$$

where Γ stands for the Gamma function.

Declaration of conflicting interests

The author declared no potential conflicts of interest with respect to the research, authorship, and/or publication of this article.

Acknowledgements

The author received no financial support for the research, authorship, and/or publication of this article.

References

1. D.E. WOLFE, J. SINGH, *Titanium carbide coatings deposited by reactive ion beam-assisted, electron beam-physical vapor deposition*, Surface and Coatings Technology, **124**, 142–153, 2000.
2. K.A. KHOR, Z.L. DONG, Y.W. GU, *Plasma sprayed functionally graded thermal barrier coatings*, Materials Letters, **38**, 437–444, 1999.
3. C.E. ROUSSEAU, H.V. TIPPUR, *Evaluation of crack tip fields and stress intensity factors in functionally graded elastic materials: cracks parallel to elastic gradient*, International Journal Fracture, **114**, 1, 87–112, 2002.
4. R.J. BUTCHER, C.E. ROUSSEAU, H.V. TIPPUR, *A functionally graded particulate composite: preparation, measurements and failure analysis*, Acta Materialia, **47**, 259–268, 1999.
5. S. SURRESH, *Graded materials for resistance to contact deformation and damage*, Science, **292**, 2447–51, 2001.
6. B. LAWN, *Indentation of Ceramics with spheres: A Century after Hertz*, Journal of the American Ceramic Society, **81**, 1977–1994, 1998.
7. M.A. GULER, F. ERDOGAN, *Contact mechanics of graded coatings*, International Journal of Solids and Structures, **41**, 3865–3889, 2004.
8. M.A. GULER, F. ERDOGAN, *The frictional sliding contact problems of rigid parabolic and cylindrical stamps on graded coatings*, International Journal of Mechanical Sciences, **49**, 161–182, 2007.
9. P. CHEN, S. CHEN, *Partial slip contact between a rigid punch with an arbitrary tip-shape and an elastic graded solid with a finite thickness*, Mechanics of Materials, **59**, 24–35, 2013.
10. X. GUO, J. FAN, H. GAO, *Mechanics of non-slipping adhesive contact on a power-law graded elastic half-space*, International Journal of Solids and Structures, **48**, 2565–2575, 2011.
11. S. BORGI, I. COMEZ, *A receding frictional contact problem between a graded layer and a homogeneous substrate pressed by a rigid punch*, Mechanics of Materials, **114**, 201–214, 2017.
12. M.A. GULER, Y. ALINIA, S. ADIBNAZARI, *On the rolling contact problem of two elastic solids with graded coatings*, International Journal of Mechanical Sciences, **64**, 62–81, 2012.
13. I. COMEZ, *Contact problem for a functionally graded layer indented by a moving punch*, International Journal of Mechanical Sciences, **100**, 339–344, 2015.
14. H.J. CHOI, G.H. PAULINO, *Thermoelastic contact mechanics for a flat punch sliding over a graded coating/substrate system with frictional heat generation*, Journal of the Mechanics and Physics of Solids, **56**, 1673–1692, 2008.
15. O. ARSLAN, S. DAG, *Contact mechanics problem between an orthotropic graded coating and a rigid punch of an arbitrary profile*, International Journal of Mechanical Sciences, **135**, 541–554, 2018.
16. T.S. VASU, T.K. BAHNDAKKAR, *Plane strain cylindrical indentation of functionally graded half-plane with exponentially varying shear modulus in the presence of residual surface tension*, International Journal of Mechanical Sciences, **135**, 158–167, 2018.

17. A. POLAT, Y. KAYA, T.S. OZSAHIN, *Analytical solution to continuous contact problem for a functionally graded layer loaded through two dissimilar rigid punches*, *Meccanica*, **53**, 3565–3577, 2018.
18. I. COMEZ, V. KAHYA, R. ERDOL, *Plane receding contact problem for a functionally graded layer supported by two quarter-planes*, *Archives of Mechanics*, **70**, 485–504, 2018.
19. R. CREMER, D. NEUSCHUTZ, *A combinatorial approach to the optimization of metastable multicomponent hard coatings*, *Surface and Coatings Technology*, **146**, 229–236, 2001.
20. V.K. GANESH, K. RAMAKRISHNA, D.N. GHISTA, *Biomechanics of bone-fracture fixation by stiffness-graded plates in comparison with stainless-steel plates*, *Biomedical Engineering Online*, **4**, 46, 2005.
21. K. RAMAKRISHNA, I. SRIDHAR, S. SIVASHANKER, K.S. KHONG, D.N. GHISTA, *Design of fracture fixation plate for necessary and sufficient bone stress shielding*, *JSME International Journal*, **47**, 1086–1094, 2004.
22. Z.N. NEJAT, M. JABBARI, M. GAHNNAD, *Elastic analysis of axially functionally graded rotating thick cylinder with variable thickness under non-uniform arbitrarily pressure loading*, *International Journal of Mechanical Sciences*, **89**, 86–99, 2015.
23. S. DAG, M.A. GULER, B. YILDIRIM, C. OZATAG, *Sliding frictional contact between a rigid punch and a laterally graded elastic medium*, *International Journal of Solids and Structures*, **46**, 4038–4053, 2009.
24. S. DAG, M.A. GULER, B. YILDIRIM, C. OZATAG, *Frictional Hertzian contact between a laterally graded elastic medium and a rigid circular stamp*, *Acta Mechanica*, **224**, 1773–1789, 2013.
25. P. CHEN, S. CHEN, J. PENGH, *Sliding contact between a cylindrical punch and a graded half-plane with an arbitrary gradient direction*, *Journal of Applied Mechanics*, **82**, 4, 2015.
26. D. DINI, D. NOWELL, *Flat and rounded fretting contact problems incorporating elastic layers*, *International Journal of Mechanical Sciences*, **46**, 1635–1657, 2004.
27. F. ERDOGAN, *Mixed boundary value problems in mechanics*, [in:] S. Nemat-Nasser [ed.], *Mechanics Today*, **4**, 1–84, 1978.
28. M.A. GULER, *Contact Mechanics of FGM Coatings*, Dissertation, Lehigh University, Bethlehem NY, 2000.

Received February 9, 2019; revised version July 17, 2019.

Published online December 3, 2019.
